AIP | Journal of Applied Physics

Oxygen induced hysteretic current-voltage characteristics of iron-phthalocyanine thin films

Soumen Samanta, Ajay Singh, A. K. Debnath, D. K. Aswal, S. K. Gupta et al.

Citation: J. Appl. Phys. **104**, 073717 (2008); doi: 10.1063/1.2990060
View online: http://dx.doi.org/10.1063/1.2990060
View Table of Contents: http://jap.aip.org/resource/1/JAPIAU/v104/i7
Published by the American Institute of Physics.

Oxygen induced hysteretic current-voltage characteristics of iron-phthalocyanine thin films

Soumen Samanta,[1] Ajay Singh,[1,a)] A. K. Debnath,[1] D. K. Aswal,[1] S. K. Gupta,[1] J. V. Yakhmi,[1] S. Singh,[2] S. Basu,[2] and S. K. Deshpande[3]
[1]*Technical Physics and Prototype Engineering Division, Bhabha Atomic Research Center, Mumbai 400 085, India*
[2]*Solid State Physics Division, Bhabha Atomic Research Center, Mumbai 400 085, India*
[3]*Department of Atomic Energy (UGC-DAE) Consortium for Scientific Research, University Grant Commission, Mumbai 400 085, India*

(Received 9 May 2008; accepted 13 August 2008; published online 3 October 2008)

Electrical transport has been investigated in amorphous and polycrystalline (α-phase) iron phthalocyanine (FePc) thin films grown by molecular beam epitaxy. Measurements carried out in the temperature range of 150–300 K showed hysteric current-voltage (*I-V*) characteristics at temperatures above 200 K. The *I-V* characteristics measured during the increasing voltage scan showed a transition from the Ohmic conduction to the trap controlled space charge limited conduction followed by a trap free conduction. During the decreasing voltage scan, trap free conduction was observed in full voltage range. The *I-V* hysteresis is attributed to the filling of deep surface traps created by chemisorbed oxygen. Amorphous films showed higher hysteresis as well as chemisorbed oxygen content. © *2008 American Institute of Physics*. [DOI: 10.1063/1.2990060]

I. INTRODUCTION

Organic semiconductors (OSCs) are attractive for electronic applications due to their low cost, simple fabrication methods, and large variation in material characteristics. These have been exploited for devices such as light-emitting diodes,[1] field-effect transistors,[2] photovoltaic cells,[3] and electronic memory.[4] In these materials, molecules are bound by weak van der Waals forces leading to narrow bands, localized charge carriers, and thermally activated charge transport. The charge transport in OSCs is not well understood and is controlled by two basic processes: (a) injection of charge carriers from electrodes into the semiconductor and (b) transport of carriers in the bulk. Depending on the semiconductor and electrode metal used, the current may be injection limited (due to the mismatch between energy levels of the electrodes and the OSC) or bulk transport limited (controlled by the intrinsic mobility of the OSC and charge traps). Both the device structure and charge traps need to be considered to understand the conduction mechanism in OSC thin films.

Hysteric *I-V* characteristics and switching at specific voltages, useful for memory devices, have been reported in different OSC thin films. Mechanisms proposed for explaining these phenomena include the formation of nanofilamentary metallic pathways,[5] conformational change,[6] charge injection control by the space charge formed at metal/polymer interface,[7] electric-field-induced charge transfer,[8,9] charge storage mechanisms (charge transfer or charge trapping),[10] redox reactions of metal ions or molecules,[11] and filling-defilling of the charge traps.[12,13] The reported mechanisms of hysteresis belong to one of the two categories. In the first category, the metallic species get embedded into an organic matrix either by deliberate inclusion or by an electromigration process. These species act as charge trapping centers, and the hysteresis is relatively insensitive to the nature of the organic material. In the second category, hysteresis is associated with the properties of the organic molecules, which includes donor-acceptor systems, redox reactions of molecules, and the conformational change of the molecules.

Metal phthalocyanine (MPc) based OSCs have received great attention due to their exceptional chemical and thermal stability. These have been widely investigated for applications in chemiresistor type gas detectors, solar cells, color filters, etc.[14] However, electrical transport in iron phthalocyanine (FePc) has not been studied in detail. This is important as FePc may also show interesting magnetic properties. Further, the effect of adsorbed oxygen (which leads to an increase in hole carrier density) on the transport properties of MPc is not well understood. In the present study, the electrical characteristics of FePc films deposited by molecular beam epitaxy have been measured and the effect of adsorbed oxygen on transport properties has been investigated. The measurements have been carried out on both amorphous and polycrystalline (α-phase) thin films as the extent of adsorbed oxygen in two types of films is quite different. The results showed hysteresis in *I-V* characteristics that was attributed to filling and defilling of surface traps created by chemisorbed oxygen similar to trap based mechanisms reported earlier.[15,16] The measurements were carried out in a planar electrode geometry to ensure that the hysteresis does not originate from metal ion incorporation in the films. The role of oxygen was confirmed by x-ray photoelectron spectroscopy (XPS) studies and measurements after repeated exposure to oxygen.

[a)]Author to whom correspondence should be addressed. Electronic mail: asb_barc@yahoo.com. Tel.: 91 22 25590441. FAX: 91 22 25505296.

II. EXPERIMENTAL

FePc films with a nominal thickness of ~100 nm were grown on glass substrates by the molecular beam epitaxy technique using a RIBER make model EVA 32 system described earlier.[17] The films were deposited using an effusion cell loaded with 97% pure α-FePc powder (Aldrich make) at substrate temperatures of 30 and 200 °C to prepare amorphous and polycrystalline films, respectively. Prior to the depositions, the evaporation source was heated at 200 °C for a prolonged period to remove the moisture and other impurities. For the determination of the deposition rate, the pressure (p) of the FePc vapors was measured at a substrate position using a flux gauge. The flux was calculated using the following relation: $F=3.52\times10^{22}(p/\sqrt{MT})$ molecules/cm^2 s, where p is the pressure in torr, M is the molecular weight of FePc (568.38), and T (in K) is the temperature of the effusion cell. The depositions were carried out at a rate of 0.07 nm/s at vacuum of better than 10^{-8} torr.

The structure of the films was determined by grazing incidence x-ray diffraction (GIXRD); measurements were carried out using Cu $K\alpha$ radiation (Seifert-XRD 3003 TT) in an out-of-plane geometry with an incidence angle of 0.1°. Neutron reflectivity (NR) measurements were carried out using a polarized neutron reflectometer installed at the Dhruva reactor in India.[18] NR data yielded information about the density, thickness, and interface roughness of the films. The morphology of the films was studied by scanning electron microscopy (SEM) images obtained using a Tescan make VEGA MV2300T/40 system. A RIBER make (model FCX 700) system was used for XPS measurements carried out using a Mg $K\alpha$ (1253.6 eV) source and a MAC-2 electron analyzer. The binding energy scale was calibrated to the Au-$4f_{7/2}$ line at 83.95 eV. For electrical measurements, two gold electrodes separated by 15 μm were evaporated using a metal mask, and silver wires were attached to the gold pads with silver paint. The I-V measurements were carried out using a Keithley make 6487 picoammeter/voltage source and a computer based data acquisition system. The measurements at low temperatures were carried out using a closed cycle cryostat.

III. RESULTS AND DISCUSSION

The SEM micrographs and GIXRD spectra of the films are shown in Fig. 1. The SEM of films deposited at 200 °C, showed densely packed crystallites similar to FePc films reported in the literature.[19] The GIXRD spectrum showed single peak (200) of α-FePc phase, indicating that the films are oriented with the a-axis normal to the substrate and have edge-on stacking of the molecules. A very high signal to noise ratio of the GIXRD peak showed good structural quality of the films. The value of the a-lattice parameter was found to be 2.54 nm, in agreement with earlier studies.[20] The SEM micrographs of the films deposited at 30 °C [inset of Fig. 1(a)] showed a very smooth texture, indicating their amorphous nature, and the same was confirmed by GIXRD spectrum shown in Fig. 1(b).

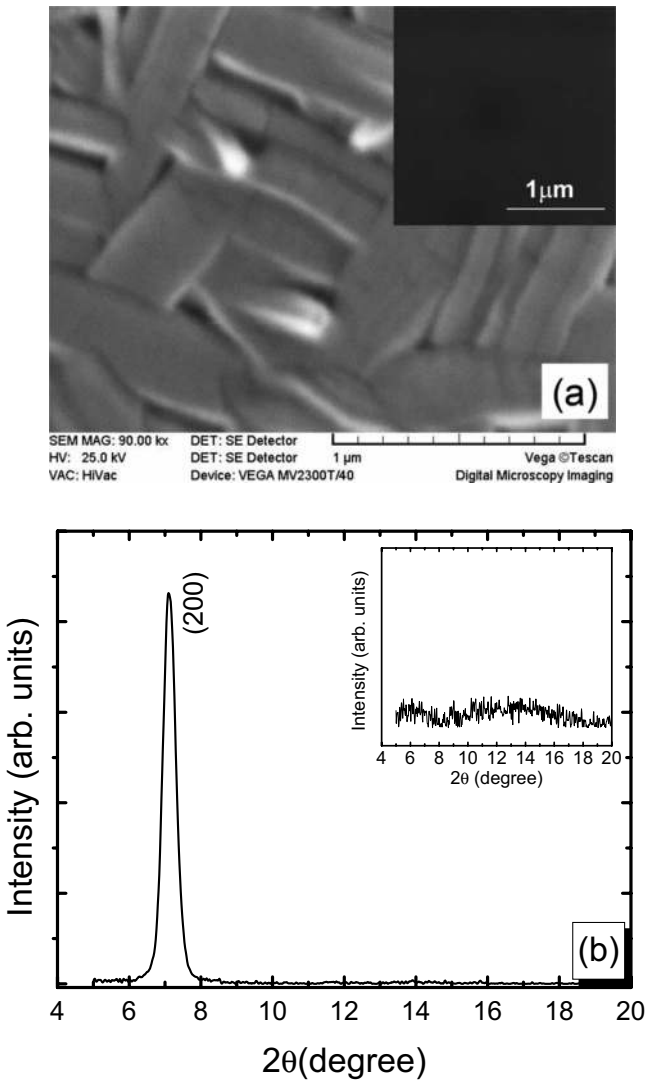

FIG. 1. (a) Scanning electron micrograph and (b) GIXRD pattern recorded for the FePc thin films deposited at 200 °C. Insets show corresponding results for room temperature deposited thin films.

NR measurements were carried out to investigate the thickness, density, and interface roughness of the grown films.[21,22] The specular reflectivity from typical amorphous and crystalline films was measured as a function of wave vector transfer Q [$Q=(4\pi/\lambda)\sin\theta$, where θ is the incident angle and λ is the wavelength of neutrons]. Specular reflectivity depends on scattering length density (SLD) $\rho(z)$ (where z is the film depth), averaged over in-plane features. NR data were fitted using a depth-dependent SLD profile $\rho(z)$ defined as $\rho(z)=\Sigma_i N_i(z)b_i$, where N_i is the (in-plane) average number density and b_i is the nuclear scattering length of individual atoms.[21,22]

Figure 2 shows the NR data for the crystalline films. Closed circles represent experimental data, and the curve shows fitting of the data using the $\rho(z)$ profile shown in the inset. The results showed a film thickness of 97 nm and $\rho(z)=4.82\times10^{-6}$ Å^{-2} (which corresponds to a density of 1.91 g/cc for FePc film). However, for amorphous films, the thickness was found to be 100 nm. The lower value of the thickness for crystalline films compared to that of amorphous films could be due to the desorption of molecules from the

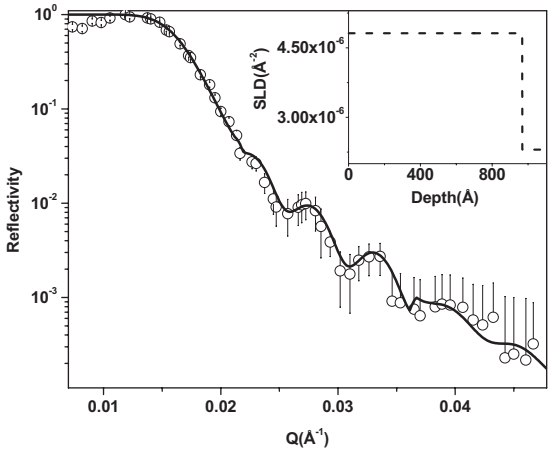

FIG. 2. NR data of the FePc thin film as a function of momentum transfer Q (Å^{-1}). Open circles are experimental points, and the solid line is the theoretical fit obtained using SLD vs depth variation shown in the inset.

hot substrate surface during deposition. For crystalline films, the results showed roughness of <20 Å for the surface and <10 Å for the film-substrate interface.

The MPc's are reported to be highly susceptible to the atmospheric oxygen, and chemisorptions of the oxygen on the central metal atoms result in the formation of charge transfer complexes. To investigate the interaction of FePc with oxygen, XPS studies were carried out. The core level XPS spectra of FePc thin films were recorded for (i) as deposited films (before exposure to atmosphere), (ii) after prolonged exposure to air (1 h), and (iii) after annealing at 200 °C for 30 min under vacuum ($\sim 10^{-6}$ torr). The results are shown in Fig. 3. As deposited films showed a single peak for Fe-$2p_{3/2}$ (at $\sim$708 eV), indicating the presence of Fe in Fe^{2+} state.[23] Similar results were obtained for the vacuum annealed sample. However, for air exposed samples, the Fe-$2p_{3/2}$ peak could be deconvoluted into two peaks with binding energies of 708 and 711 eV corresponding to Fe^{2+} and Fe^{3+} states, respectively.[24] The presence of Fe^{3+} states at the surface is attributed to the formation of the charge transfer complex between Fe and chemisorbed oxygen. The formation of the Fe–O charge transfer complex was further confirmed by the analysis of the O-1*s* spectra. For air exposed films, the O-1*s* spectrum showed two components at binding energies of 531 and 533 eV attributed to physisorbed and chemisorbed oxygen, respectively.[24–26] Fresh samples did not show the presence of oxygen, as expected for films deposited under ultrahigh vacuum conditions while vacuum annealed films exhibited the presence of physisorbed oxygen only. Thus the XPS data clearly show that on exposure to oxygen, Fe^{2+} is oxidized to Fe^{3+}, and the chemisorbed oxygen desorbs on vacuum annealing, which is in agreement with reported literature.[27] For air exposed samples, the Fe^{3+}/Fe^{2+} ratio was found to be 0.94 and 0.78 for amorphous and crystalline samples, respectively, indicating a stronger interaction of amorphous samples. This is attributed to the high defect density in amorphous films.

To understand the influence of chemisorbed oxygen on the charge transport, *I-V* characteristics were measured for vacuum annealed polycrystalline films (measured in vacuum

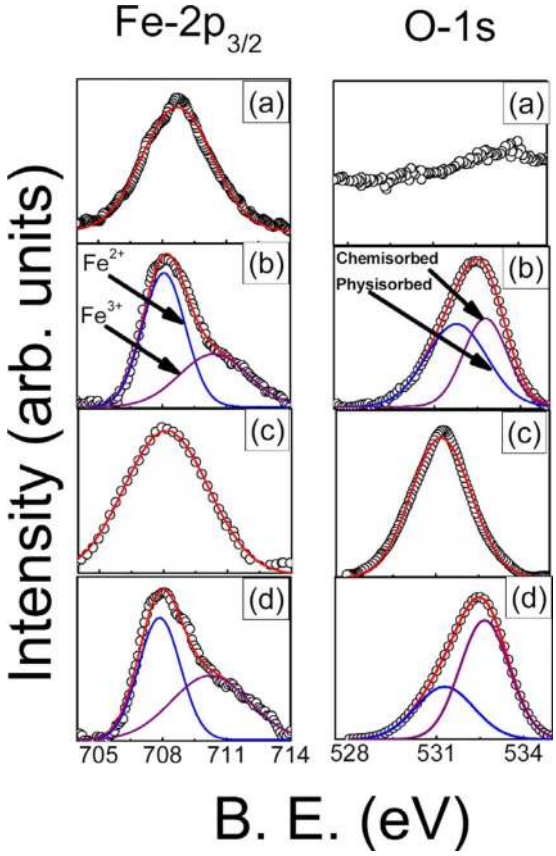

FIG. 3. (Color online) Core level Fe-$2p_{3/2}$ and O-1*s* XPS spectra of (a) as prepared (*in situ* measurement), (b) air exposed, and (c) vacuum annealed FePc films in crystalline form. (d) shows XPS spectra for amorphous films after exposure to air.

at room temperature) and those exposed to atmosphere for short (<5 min) and long (1 h) times (measurement in air), and the results are shown in Fig. 4. It is seen that the *I-V* characteristics for vacuum annealed films exhibit an Ohmic behavior and do not have hysteresis, while air exposed films

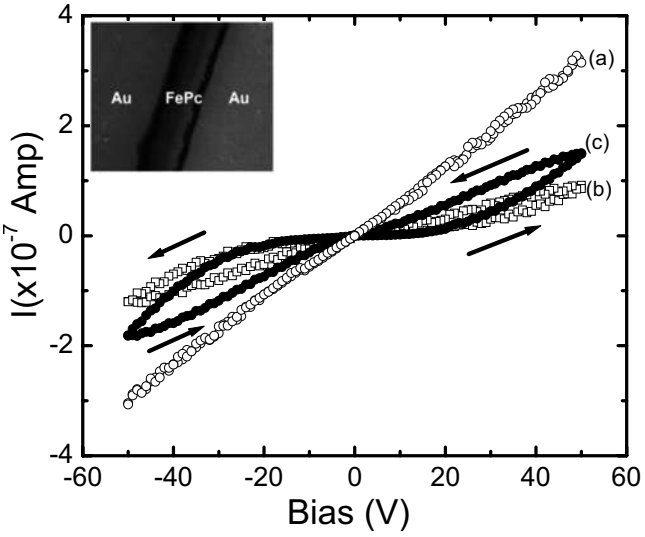

FIG. 4. *I-V* characteristics recorded at 300 K after (a) vacuum annealing and (b) short and (c) long time exposure to atmosphere. The inset shows the SEM micrograph of the planar Au/FePc/Au structure used for measurements.

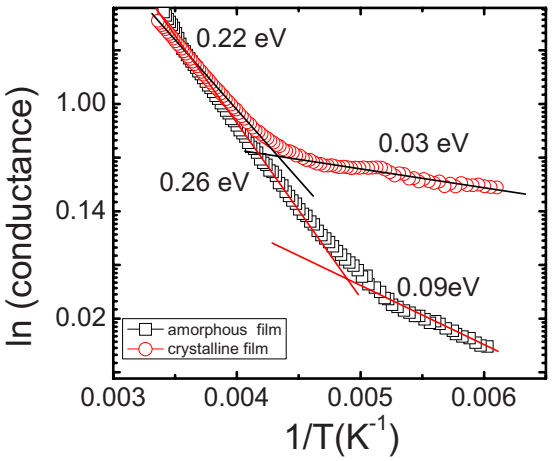

FIG. 5. (Color online) Temperature dependence of the conductance recorded for amorphous and crystalline FePc films.

show both hysteresis and nonlinear characteristics. Further, the hysteresis increases with an increase in air exposure time. As demonstrated by XPS studies, the films adsorb oxygen on exposure to atmosphere, and therefore we believe that the presence or absence of the hysteresis is related to the chemisorbed oxygen. We also see (Fig. 4) that the vacuum annealed films have higher conductivity compared to air exposed films. This indicates that in addition to hole doping (as suggested by the oxidation of Fe^{2+} to Fe^{3+}), the chemisorbed oxygen creates surface traps, which localize the charge. Therefore, both hole doping and charge localization need to be considered to understand the electrical properties of these films.

To further understand the conduction mechanism, the conductivity of air exposed films was measured (at a voltage of 50 V) as a function of temperature, and the results are presented in Fig. 5. A change in conduction mechanism is evident at a temperature of ~200 K. Fitting of the temperature dependence of conductance to the thermally activated hopping model, $\sigma=\sigma_0 \exp(\Delta E/kT)$, reveals two activation energies, $\Delta E_1=0.22$ eV ($T>220$ K) and $\Delta E_2=0.03$ eV ($T<220$ K) for crystalline films and $\Delta E_1=0.26$ eV ($T>200$ K) and $\Delta E_2=0.09$ eV ($T<200$ K) for amorphous films. The presence of two different activation energies indicates the possibility of two different types of charge trap states in the films: (i) surface traps arising due to chemisorbed oxygen and (ii) bulk traps arising due to impurity/structural defects. The first activation energy (ΔE_1) is very close to the value of 0.26 eV reported for the MPc-oxygen interaction.[27] The lower activation energy effective at temperatures <200 K is attributed to bulk traps.

The hysteresis in the *I-V* characteristics was studied as a function of temperature (for air exposed samples), and the results obtained in the voltage range of ±50 V are shown in Fig. 6. It is seen that hysteresis is higher for amorphous films than for crystalline films, in agreement with XPS data, indicating higher chemisorbed oxygen in this case. Further, the hysteresis reduces at lower temperatures (150 K), and *I-V* characteristics are linear (seen by replotting data in the linear scale, not shown here), indicating that traps are ineffective at low temperatures due to high activation energy.

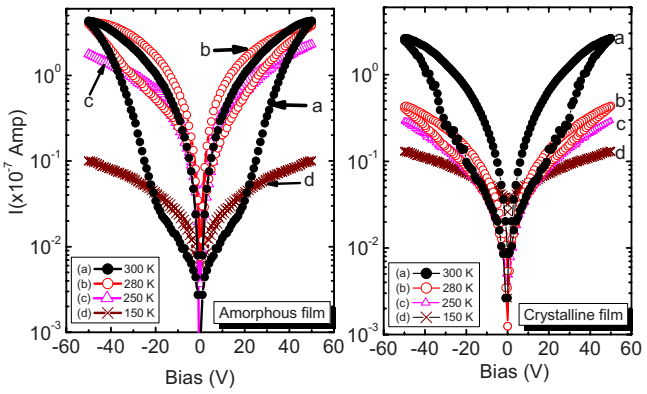

FIG. 6. (Color online) Temperature dependence of *I-V* characteristics for amorphous and crystalline FePc films.

To understand the charge transport mechanism, we have replotted the room temperature *I-V* characteristics in the log-log scale, and the results are shown in Fig. 7 for both crystalline and amorphous films. A power law behavior of *I-V* characteristics ($I\sim V^{\alpha}$) is observed in different regions, with exponent (α) increasing (for the increasing voltage scan) from ~1 at low voltages to a value of ~5 at a voltage of about 25 V and finally to 2 at higher voltages. For the reducing voltage scan, the exponent has a constant value of 2 at all voltages. The value of the exponent is an indication of the conduction mechanism, and its variations indicate a crossover in conduction mechanisms as a function of voltage. For voltages <10 V, $\alpha\sim 1$ and linear *I-V* may be described by[28]

$$J = n_0 e \mu E, \tag{1}$$

where J is the current density, n_0 is the concentration of thermally generated holes, e is the electronic charge, μ is the hole mobility, and E is the electric field. In the Ohmic regime, the density of the injected charge carriers is much less than the thermally generated carrier density leading to a linear behavior. Room temperature values of n_0 determined from Eq. (1) (using typical mobility values of 7×10^{-5} m^2 V^{-1} s^{-1} reported for MPc) are given in Table I for both types of films.[28,29]

For the voltage range of 10–20 V, characteristics ($\alpha\sim 2$) indicate space charge limited conduction (SCLC).[28] SCLC occurs if the injection electrode forms an Ohmic contact with the organic film. Due to the presence of a very small energy barrier of 0.2 eV at the Au/FePc interface, an Ohmic contact is expected.[30] At sufficiently high voltages,

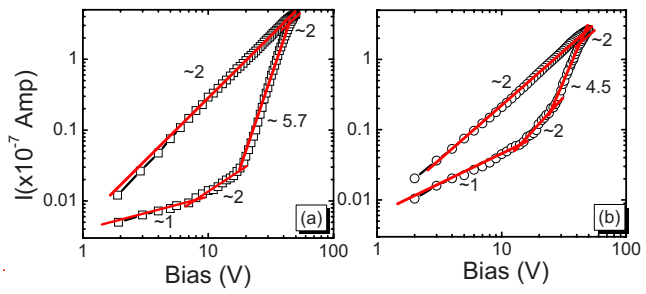

FIG. 7. (Color online) *I-V* characteristics for (a) amorphous and (b) crystalline films recorded at 300 K in the log-log scale.

TABLE I. Parameters of the FePc film determined from *I-V* characteristics.

Sample	Hole concentration (n_0)	Trap characteristic temperature (T_t)	Total surface trap density (N_t)	Surface trap concentration per unit energy at the valence band edge (P_0)
Amorphous	6.4×10^{17} m^{-3}	1410 K	1.03×10^{23} m^{-3}	5.3×10^{42} J^{-1} m^{-3}
Crystalline	2×10^{18} m^{-3}	1050 K	3.9×10^{21} m^{-3}	2.7×10^{41} J^{-1} m^{-3}

the injected carrier concentration exceeds that of thermally generated carriers, and the SCLC current becomes dominant. The existence of traps within the organic film has the effect of localizing a large proportion of charge carriers. If the traps are shallow and located at a discrete energy level above the valence band edge, the current is given by[28]

$$J=\frac{9\varepsilon\mu V^2}{8d^3}\theta, \tag{2}$$

where d is the electrode separation, ε is the permittivity of the FePc, and θ is given by $\theta=p/(p+p_t)$, where p is the density of free holes and p_t is the density of trapped holes. Therefore, the observed slope of 2 in the 10–20 V bias range is attributed to SCLC with the shallow discrete traps.

For the voltage range of 20–40 V, the current rises rapidly, and $\alpha\sim5.7$ for amorphous films and ~4.5 for crystalline films. The higher value of exponent (>2) suggests a SCLC mechanism in the presence of deep traps (i.e., surface traps), which are distributed exponentially in energy above the valence band edge. In this regime the *I-V* characteristics may be described by[28,29,31]

$$J=e\mu N\left(\frac{\varepsilon}{eP_0kT_t}\right)^l\frac{V^{l+1}}{d^{2l+1}}, \tag{3}$$

where N is the effective density of states at the valence band edge, P_0 is the trap density per unit energy range at the valence band edge, and l is the ratio T_t/T, where T is the absolute temperature and T_t is the temperature characterizing the trap distribution.[28] Using reported values of N (10^{27} m^{-3}) and ε (2.43×10^{-5} F/m) for MPc, values of T_t and P_0 were determined from Eq. (3) and are given in Table I. The total concentration of surface traps (N_t) can be determined from the value of P_0 and T_t using the following equation:[28]

$$N_t=P_0kT_t. \tag{4}$$

The value of N_t determined in this manner is also listed in Table I.

The values of n_0, T_t, N_t, and P_0 are within the range of reported values for various MPc's.[28] It may be noted that surface trap density is higher for amorphous films than for crystalline films. This is in agreement with the higher concentration of Fe^{3+}/Fe^{2+} for the amorphous films.

For voltages >40 V, the current rises slowly and the exponent again reduces to ~2. It is attributed to filling of all traps so that the sample behaves like a trap free sample.[28,29] In this regime, the *I-V* characteristic follows Child's law,[31]

$$J=\frac{9\varepsilon\mu V^2}{8d^3}. \tag{5}$$

Summing up, as the voltage is scanned from 0 to 50 V, the carrier transport mechanism changes from Ohmic to SCLC controlled by shallow traps to SCLC controlled by traps exponentially distributed in energy and finally to SCLC controlled by Child's law. On the reverse scan, the films show high conductance with $\alpha\sim2$, indicating that trapped carriers are not released. Thus the film behaves like a trap free sample, and the *I-V* characteristic follows Child's law. The

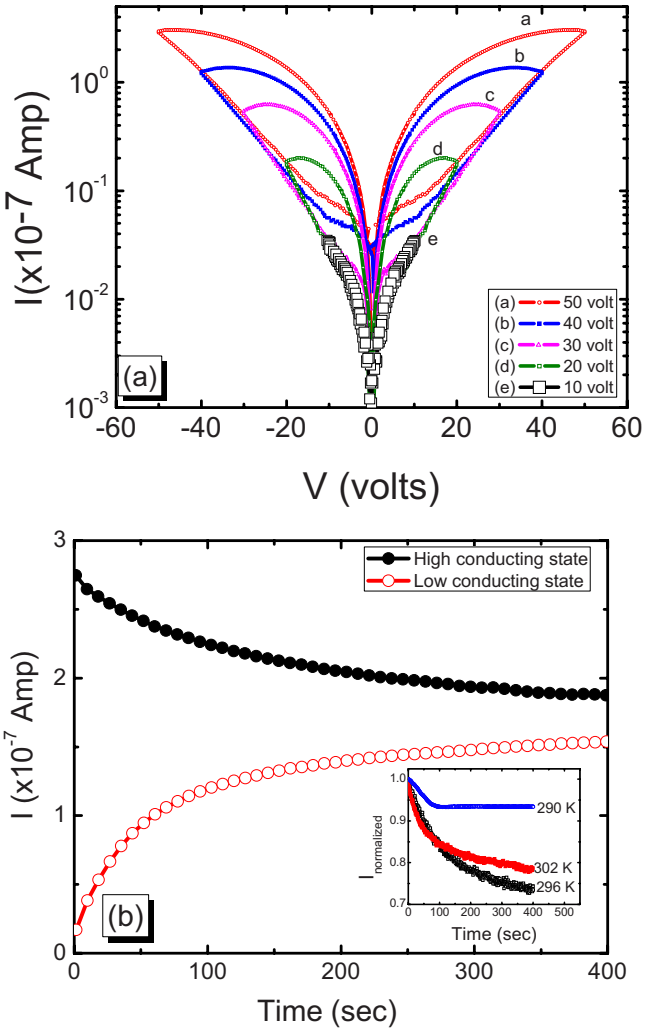

FIG. 8. (Color online) (a) *I-V* characteristics recorded at 300 K with different values of maximum voltage bias. (b) Time dependence of the current recorded for high and low conducting states measured at a voltage of 30 V. The inset shows the time dependence of the current starting from the high conducting state at different temperatures.

data show that hysteresis arises from trapping of carriers on the application of voltage (leading to high conductivity state) and their release on the reduction of voltage (yielding lower conductivity state).

In order to investigate the feasibility of the observed hysteresis for the memory effect, we have measured the maximum bias dependence of the *I-V* characteristics, and the results are shown in Fig. 8(a). Clearly, the hysteresis is absent for applied voltages <10 V and increases with voltage. To investigate the time dependence of different states and memory effect, we define the low conductivity state as 0 and the high conductivity state as 1. We write 0 and 1 by the application of zero and +50 V, respectively, for a time period of 100 s. After writing 0 or 1, we read the state by a continuous application of a voltage of +30 V. The results are shown in Fig. 8(b). The ratio of currents in 1 and 0 states reduces from the initial value of ~ 19 to 1.4 after 400 s. The decrease in current ratio is attributed to the relaxation of trapped charge carriers. To investigate the relaxation mechanism, we studied the time dependence of current (at the applied voltage of 30 V) starting from the high conductivity state at different temperatures, and the results are shown in the inset in Fig. 8(b). It is observed that the relaxation rate increases with temperature, indicating that the relaxation process is predominantly thermally activated. The observed memory effect was found to be repeatable and reproducible.

IV. CONCLUSIONS

We have studied the current-voltage (*I-V*) characteristics of the amorphous and crystalline iron phthalocyanine (FePc) thin films grown by molecular beam epitaxy. By carrying out the room temperature *I-V* measurements on vacuum annealed and air exposed samples, we have demonstrated that the *I-V* hysteresis in FePc films is intimately related to the filling and defilling of deep surface traps created by chemisorbed oxygen. The presence of chemisorbed oxygen has been confirmed by the XPS. Room temperature *I-V* characteristics showed higher hysteresis for amorphous films than for crystalline films, indicating higher density of surface sites for chemisorption in amorphous films. The study indicates that the FePc films may be utilized in memory devices.

[1]C. W. Tang and S. A. Van Slyke, Appl. Phys. Lett. **51**, 913 (1987); J. H. Burroughes, D. D. C. Bradley, A. R. Brown, R. N. Marks, K. Mackay, R. H. Friend, P. L. Bums, and A. B. Holmes, Nature (London) **347**, 539 (1990).
[2]F. Garnier, R. Hajlaoui, A. Yassar, and P. Srivastava, Science **265**, 1684 (1994).
[3]N. S. Sariciftci, L. Smilowitz, A. J. Heeger, and F. Wudl, Science **258**, 1474 (1992).
[4]L. Ma, J. Liu, S. Pyo, and Y. Yang, Appl. Phys. Lett. **80**, 362 (2002); J. C. Scott, Science **304**, 62 (2004).
[5]D. Tondelier, K. Lmimouni, and D. Vuillaume, Appl. Phys. Lett. **85**, 5763 (2004).
[6]A. K. Mahapatro, R. Agrawal, and S. Ghosh, J. Appl. Phys. **96**, 3583 (2004).
[7]H. S. Majumdar, A. Bandyopadhyay, A. Bolognesi, and A. J. Pal, J. Appl. Phys. **91**, 2433 (2002); H. S. Majumdar, A. Bolognesi, and A. J. Pal, Synth. Met. **140**, 203 (2004).
[8]Q. D. Ling, Y. Song, S. J. Ding, C. X. Zhu, D. S. H. Chan, D. L. Kwong, E. T. Kang, and K. G. Neoh, Adv. Mater. (Weinheim, Ger.) **17**, 455 (2005).
[9]J. Ouyang, C.-W. Chu, C. Szmanda, L. Ma, and Y. Yang, Nature Mater. **3**, 918 (2004); J. Ouyang, C.-W. Chu, D. Sievers, and Y. Yang, Appl. Phys. Lett. **86**, 123507 (2005).
[10]R. J. Tseng, J. Huang, J. Ouyang, R. B. Kaner, and Y. Yang, Nano Lett. **5**, 1077 (2005); L. D. Bozano, B. W. Kean, M. Beinhoff, K. R. Carter, P. M. Rice, and J. C. Scott, Adv. Funct. Mater. **15**, 1933 (2005).
[11]S. P. Koiry, D. K. Aswal, A. K. Chauhan, V. Saxena, S. K. Nayak, S. K. Gupta, and J. V. Yakhmi, Chem. Phys. Lett. **453**, 68 (2008).
[12]A. K. Chauhan, D. K. Aswal, S. P. Koiry, S. K. Gupta, and J. V. Yakhmi, Phys. Status Solidi A **205**, 373 (2008); A. K. Chauhan, D. K. Aswal, S. P. Koiry, S. K. Gupta, J. V. Yakhmi, C. Suergers, D. Guerin, S. Lenfant, and D. Vuillaume, Appl. Phys. A: Mater. Sci. Process. **90**, 581 (2008).
[13]W. Tang, H. Shi, G. Xu, B. S. Ong, Z. D. Popovic, J. Deng, J. Zhao, and G. Rao, Adv. Mater. (Weinheim, Ger.) **17**, 2307 (2005); J. Chen and D. Ma, Appl. Phys. Lett. **87**, 023505 (2005).
[14]G. Guillaud, J. Simon, and J. P. Germain, Coord. Chem. Rev. **178–180**, 1433 (1998).
[15]B. Mukherjee and A. J. Pal, Org. Electron. **8**, 584 (2007).
[16]B. Mukherjee, A. K. Ray, A. K. Sharma, M. J. Cook, and I. Chambrier, J. Appl. Phys. **103**, 074507 (2008).
[17]A. K. Debnath, N. Joshi, K. P. Muthe, J. C. Vyas, D. K. Aswal, S. K. Gupta, and J. V. Yakhmi, Appl. Surf. Sci. **243**, 220 (2005); D. K. Aswal, K. P. Muthe, N. Joshi, A. K. Debnath, S. K. Gupta, and J. V. Yakhmi, J. Cryst. Growth **256**, 201 (2003); A. K. Debnath, N. Joshi, D. K. Aswal, S. K. Deshpande, S. K. Gupta, and J. V. Yakhmi, Solid State Commun. **142**, 200 (2007).
[18]S. Basu and S. Singh, J. Neutron Res. **14**, 109 (2006).
[19]W. Y. Tong, A. B. Djurisic, M. H. Xie, A. C. M. Ng, K. Y. Cheung, W. K. Chan, Y. H. Leung, H. W. Lin, and S. Gwo, J. Phys. Chem. B **110**, 17406 (2006).
[20]M. M. El-Nahass, F. S. Bahabri, A. A. AL Ghamdi, and S. R. Al-Harbi, Egypt. J. Solids **25**, 307 (2002).
[21]S. J. Blundell and J. A. C. Bland, Phys. Rev. B **46**, 3391 (1992).
[22]C. F. Majkrzak, Physica B (Amsterdam) **173**, 75 (1991).
[23]G. V. Ouedraogo, D. Benlian, and L. Porte, J. Chem. Phys. **73**, 642 (1980).
[24]J. F. Moulder, W. F. Stickle, P. E. Sobol, and K. D. Bombson, *Handbook of X-Ray Photoelectron Spectroscopy* (Physical Electronics, Minnesota, 1995).
[25]T. Kawabe, K. Tabata, E. Suzuki, Y. Yamaguchi, and Y. Nagasawa, J. Phys. Chem. B **105**, 4239 (2001).
[26]A. K. Hassan and R. D. Gould, J. Phys.: Condens. Matter **1**, 6679 (1989).
[27]I. Zhivkov, E. Spassova, D. Dimov, and G. Danev, Vacuum **76**, 237 (2004).
[28]R. D. Gould, Coord. Chem. Rev. **156**, 237 (1996).
[29]T. D. Anthopoulos and T. S. Shafai, J. Vac. Sci. Technol. A **20**, 295 (2002).
[30]A. K. Mahapatro and S. Ghosh, J. Appl. Phys. **101**, 034318 (2007).
[31]D. S. Shang, L. D. Chen, Q. Wang, W. Q. Zhang, Z. H. Wu, and X. M. Li, Appl. Phys. Lett. **89**, 172102 (2006).